In-Situ EMF and Safety Assessment of an EV Wireless Charging System

Cristian Giovanni Colombo
Department of Energy
Politecnico di Milano
Milan, Italy
cristiangiovanni.colombo@polimi.it

Harutaka Suzuki
Faculty of Systems Design
Tokyo Metropolitan University
Tokyo, Japan
suzuki-harutaka@ed.tmu.ac.jp

Ryosuke Ota
Faculty of Systems Design
Tokyo Metropolitan University
Tokyo, Japan
r_ota@tmu.ac.jp

Michela Longo
Department of Energy
Politecnico di Milano
Milan, Italy
michela.longo@polimi.it

Giuseppe Mastroviti
A35 Brebemi SPA
Chiari, Italy
giuseppe.mastroviti@brebemi.it

Gianfermo Lupi
A35 Brebemi SPA
Chiari, Italy
gianfermo.lupi@brebemi.it

***Abstract*—This paper presents an in-situ characterization and safety assessment of the ElectroMagnetic Field (EMF) generated by an Electric Vehicle (EV) wireless power transfer system installed at the "Arena del Futuro" test track. The goal is to develop and apply a unified, standards-aligned measurement protocol for both static and dynamic operating conditions, enabling quantitative evaluation of magnetic flux density metrics and uncertainty. Field mapping was conducted inside and outside the vehicle, including dynamic tests with two drivers to assess repeatability and identify geometric hot-spots. Results show that all measured magnetic flux densities remain well below ICNIRP/IEEE exposure limits and comply with EV-specific standards (SAE J2954, IEC 61980). This work provides a replicable framework for real-world EMF compliance in DWPT installations.**

***Index Terms*—Wireless Power Transfer, Dynamic Wireless Power Transfer, Magnetic Flux Density, Safety Standards, Electric Vehicles**

Nomenclature

Symbol [Unit]	Definition
B_x, B_y, B_z [μT]	Orthogonal components of magnetic flux density
$\|B\|(t)$ [μT]	Resultant magnetic flux density $\sqrt{B_x^2 + B_y^2 + B_z^2}$
$B_{\min}$ [μT]	Minimum value of the magnetic field resultant $\|B\|(t)$ within the measurement window
B_{peak} [μT]	Maximum value of the resultant $\|B\|(t)$ within the measurement window
B_{mean} [μT]	Arithmetic mean of $\|B\|(t)$ over N samples
std [μT]	Sample standard deviation of $\|B\|(t)$
$B_{\text{RMS,avg}}$ [μT]	Average RMS magnetic flux density calculated over sliding RMS windows
t_i [s]	Timestamp of the i-th sample
N [–]	Number of samples within a measurement window
A,B,C,D,E,F,G,H	Measurement point identifiers
D1, D2	Driver identifiers for dynamic tests

This study was carried out within the MOST – Sustainable Mobility Center and received funding from the European Union Next-GenerationEU (PIANO NAZIONALE DI RIPRESA E RESILIENZA (PNRR) – MISSIONE 4 COMPONENTE 2, INVESTIMENTO 1.4 – D.D. 1033 17/06/2022, CN00000023). This manuscript reflects only the authors' views and opinions, neither the European Union nor the European Commission can be considered responsible for them.

I. Introduction

With the spread of Electric Vehicles (EVs), the societal deployment of Wireless Power Transfer (WPT) which enables contactless, automated charging has advanced. In particular, dynamic wireless power transfer (DWPT), wherein primary coils are embedded in the road to supply power continuously while driving, is regarded as promising for reducing the burden of charging behavior and improving utilization rates. For the introduction of such WPT systems, safety assessment grounded in the reference levels and dosimetric quantities of low-frequency ElectroMagnetic Fields (EMF) is essential. Specifically, international exposure guidelines (ICNIRP/IEEE) organize reference levels for the general public [1]–[3], and design requirements for EV wireless charging have been developed under SAE J2954 and IEC 61980 [4], [5].

Regarding the generation mechanisms and mitigation of leakage magnetic fields, prior studies have clarified near-pad field distributions by finite-element analysis and shown that radiation can be suppressed through vehicle-body shielding and pad-structure design [6]. Beyond passive measures using ferrite and conductive plates, active measures that apply counter-phase magnetic fields via auxiliary coils are under investigation, with concurrent pursuit of compatibility with efficiency [7]–[9].

Accordingly, the present study targets the EV-oriented WPT system installed at the "Arena del Futuro" test track on the BreBeMi expressway, with the objectives of: (1) Unified, standards-aligned measurement protocol for EV WPT at the real-case study Arena del Futuro, covering static and dynamic operation with consistent reconstruction of $|B|(t)$, no peak clipping, and reporting of $B_{\min}$, B_{mean}, B_{peak}, std and $B_{\text{RMS,avg}}$; (2) In-situ field mapping and analysis at representative external and internal locations, plus supplied/unsupplied dynamic runs with two drivers, including windowed-RMS variability and uncertainty elements, thereby quantifying geometric hot-spots, dispersion and driver repeatability under practical considera-

979-8-3315-8138-1

tions; (3) Safety evaluations with respect to ICNIRP/IEEE and EV specific standards, such as SAE J2954 and IEC 61980. No pronounced transient or anomalous behavior were observed, and magnetic flux densities remained within applicable limits, providing actionable inputs for compliance checks and operational design. The work follows this structure: after the introduction section, Section II collects the methodology, where the system configuration and the test environment are defined at the beginning. Then data processing and analysis setup is described. Section III collects the measurements results for both static and dynamic tests. Results discussion is included in this section. Finally, Section IV collects the conclusions of the work, highlighting the relevance of the presented study.

II. Methodology

The experimental setup and procedures for evaluating the electromagnetic performance and biological safety of a WPT system conducted using a Fiat 500e EV at the "Arena del Futuro" test facility located on the BreBeMi highway in Italy are described. Measurements are collected through the Wavecontrol SMP2-5G, which is equipped with the WP400 probe for measuring magnetic fields from 1 Hz to 400 kHz. The EV used and the measurement device for magnetic flux density are reported in Fig. 1.

Fig. 1. Fiat 500e used in the measurements and magnetic flux measurement device.

A. System Configuration and Test Environment

The system used at the Arena del Futuro is a WPT system with compensation architecture. The system draws power from a 1 MW power transformer cabin, with conversion to 600 V DC. Subsequently, the inverters allow conversion to AC at a resonance frequency f_0 = 86 kHz for power transfer between the Tx and Rx coils, respectively transmitter and receiver. To ensure the effective transfer of 10 kW, compensation structures are located on both the primary and secondary sides between the converters and the coils. Finally, there is a rectifier to supply the EV battery with DC current. The architecture described is shown in Fig. 2 [10].

The tests were carried out in different positions simulating the presence of people inside and outside the vehicle, as shown in Fig. 3. The positions highlighted in red are outside the vehicle and serve to highlight the maximum magnetic flux density detected near the car. This serves to simulate the presence of a person. A magnetic flux density below the tolerance threshold defined by the standards will highlight the compatibility of the WPT system for use in parking areas. The same measurement was repeated at the points highlighted in green, inside the vehicle. The positions of interest are those resting on the seats and those on the floor where the measured field is expected to be maximum, considering the proximity of the coils. Finally, having highlighted internal point C as critical given its proximity to the receiver, measurements at this point were also repeated in dynamic mode.

B. Data Processing and Analysis

The raw files extracted from the measuring instruments were imported and normalized into numerical form. The time series were then reconstructed from the timestamps. No filters were applied that would alter the content at f_0. When the three axial components were available, the resulting field was reconstructed following (1).

$$|B|(t) = \sqrt{B_x^2(t) + B_y^2(t) + B_z^2(t)} \tag{1}$$

The indicators reported in Table **??** were calculated for each of the positions [11]. Considering t_n the time of the n-th sample and N the total number of samples, the metric are defined as (2)-(5).

$$B_{\text{min}} = \min |B|(t) \tag{2}$$

$$B_{\text{peak}} = \max |B|(t) \tag{3}$$

$$B_{\text{mean}} = \frac{1}{N} \sum_{n=1}^{N} |B|(t_n) \tag{4}$$

$$\text{std} = \sqrt{\frac{1}{N-1} \sum_{n=1}^{N} \left(|B|(t_n) - B_{\text{mean}}\right)^2} \tag{5}$$

Finally, the average RMS window value is defined through (6).

$$B_{\text{RMS,avg}} = \frac{1}{M} \sum_{m=1}^{M} B_{\text{RMS}} \tag{6}$$

Any obviously corrupted samples (non-numeric) were excluded. No clipping was applied to the peaks, so that B_{peak} reflects the actual observed maxima [12], [13].

979-8-3315-8138-1

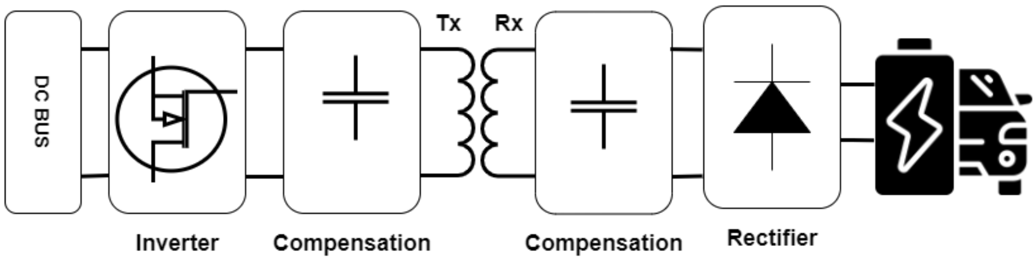

Fig. 2. Equivalent circuit representation of charging system.

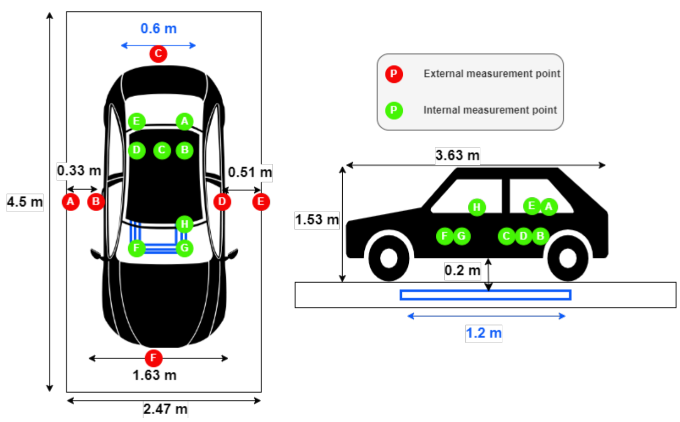

Fig. 3. Environment of measurement collection.

III. Results and Discussion

This section shows the results of B_{min}, B_{mean}, B_{peak}, std and $B_{\text{RMS,avg}}$ obtained from the uniform processing flow applied to all reconstructed acquisitions. The analysis covers static measurements outside and inside the vehicle, followed by dynamic measurements inside the vehicle taken by two drivers on both powered and unsupplied lanes. The measurements will identify key and repeatable aspects for the experimental campaigns, highlighting critical points for further sensorisation. Finally, the results will be compared with the relevant standards to ensure the safety of the charging system. Fig. 4 highlights the results obtained from the measurements performed in the positions outside of the vehicle.

The results show a marked spatial dependence of the magnetic flux density levels measured along the perimeter of the vehicle. The averages B_{mean} vary from 3.698 to 28.559 μT, with the maximum values recorded at position D, near the vehicle (B_{mean} = 28.559μT, B_{peak} = 28.635μT) and more modest values in F, corresponding to the front of the vehicle (B_{mean} = 3.698μT, B_{peak} = 3.717μT). The dispersion is limited, the standard deviation (std) is between 0.008 and 0.065, with coefficients of variation typically less than 0.5% (i.e. A: 0.020/5.338=0.37%, D: 0.043/28.559=0.15%). The relative difference between peak and average magnetic flux density is also small (≤0.8%), indicating stable operating conditions and constant transmitter-receiver coupling over time. The parameter $B_{\text{RMS,avg}}$ consistently follows the ranking of points (e.g., D: 19.229μT, B: 16.415μT, C: 13.362μT), confirming that the geometric positions closest to the coupling, or along the prevailing field line, have higher levels.

Then, Fig. 4b reports the results obtained from the measurements performed in the positions inside of the vehicle.

The measurements taken inside the vehicle show significantly lower levels than outside. B_{mean} ranges from 0.497 (B) to 1.045 (F), while B_{peak} ranges from 0.523 to 1.053. The standard deviation remains low (0.005÷0.0169), but the coefficients of variation are higher than outside (typically 0.5÷3%), and the relative peak-to-average difference can reach 5÷6% in some positions (H and B). This behavior is compatible with slight local dynamics in the passenger compartment (wiring, surrounding metal masses, non-perfectly uniform shielding conditions), even in an overall stationary regime. Here too, $B_{\text{RMS,avg}}$ maintains the same hierarchy, with the maximum at point F ($B_{\text{RMS,avg}}$ = 0.624μT) consistent with the intuition that the regions closest to the floor or return flow paths have higher levels.

Overall, the data indicate a marked gradient between the exterior and interior. The interior values are one order of magnitude lower than the exterior values. The maximum peaks are B_{peak} = 28.635μT externally, while they are limited to B_{peak} = 1.053μT internally, confirming the combined effectiveness of distance, body shielding, and coupling geometry in containing the field in the passenger compartment. The low variability outside (<0.5%) suggests that the measurement setup maintained repeatable conditions and that points A-F intercept relatively stable coupling configurations. Inside, although at lower levels, there is greater relative variability (up to 3%), due to the greater sensitivity of the small-scale field to internal elements, such as coatings and structures, and to the position of the sensor, respectively on the seat or on the floor.

The external map clearly highlights geometric hot-spots near the charging vehicle (external points D and B), where the field is strongest. This is useful for planning sensor placements and guiding coupler layout optimizations. Furthermore, the systematic reduction of flux levels in the passenger compartment confirms that the shielding and mechanical integration choices are effective. The internal points with relatively higher values (F) are natural candidates for possible refinements, with possible local shielding. Finally, the fact that B_{peak} slightly

979-8-3315-8138-1

exceeds B_{mean} on the outside and by a few percentage points on the inside indicates the absence of pronounced transients related to power-ups or power-downs that alter the statistics. The time series and histograms in Fig. 4 confirm the narrow distribution, with no anomalous tails. For stationary charging, the standard deviation value std applied to B_{rms} is not calculated as it is less than 1%.

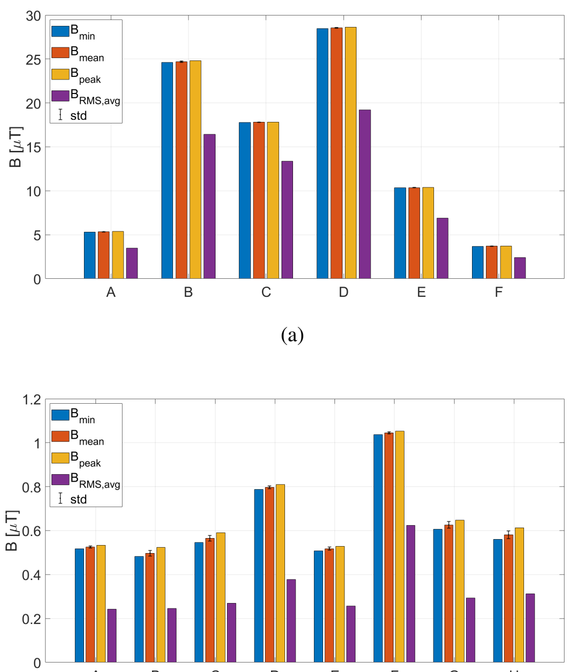

Fig. 4. Bar-chart of magnetic field metrics for static wireless charging: (a) external and (b) internal. Error bars indicate ± one standard deviation.

The same measurements were then repeated in the internal point C for the 1 km dynamic section with two different drivers, in order to broaden the spectrum of measurements taken. Fig. 5 shows the results obtained during this phase.

The dynamic measurements show a clear separation between the energized and non-energized sections of the track, with consistent differences across all metrics considered. In the supplied sections, the average magnetic field B_{mean} measures between 5.43 and 6.45 μT, while in the unsupplied sections it ranges between 0.28 and 30 μT. The peaks (B_{peak}) also follow a similar trend: 12.38÷12.85 μT in the supplied sections, compared to 0.73÷1.11 in the unsupplied sections. The $B_{\text{RMS,avg}}$ metric confirms the trend, ranging from 1.885÷2.116 μT in the supplied section to 0.098÷0.105 μT in the unsupplied sections. These ratios clearly quantify the impact of road section powering on the field distribution at the edge. The variation in std is between 2.627÷3.463 μT on the supplied sections and 0.070÷0.101 μT on the unsupplied sections, highlighting greater intermittency along the supplied section, consistent with the succession of active coils and variations in the vehicle's trajectory. The std, rms dispersion is also marked, ranging from 0.920÷1.185 μT on the supplied sections to 0.028÷0.029 μT on the unsupplied sections. Furthermore, it can be seen that D 2 shows a higher B_{mean} and also a slightly higher $B_{\text{RMS,avg}}$, but a lower std than D1. This indicates a higher but more regular average level, linked to better lateral centering of the supplied lane and a more constant speed. The peaks obtained by drivers, on the other hand, are comparable and can be associated with close passages over individual coils. In the unsupplied sections, all metrics are at least one order of magnitude lower than their powered counterparts and with lower dispersion. This level represents a useful baseline for comparison and confirms that the main contributions in dynamic conditions come from interaction with the powered infrastructure.

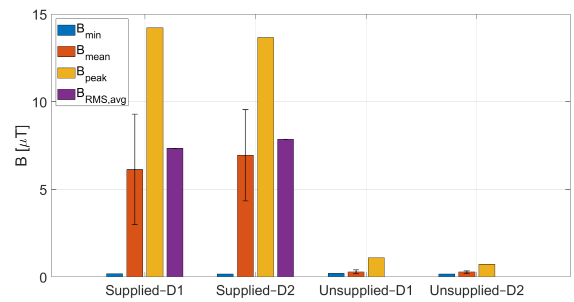

Fig. 5. Bar-chart of magnetic field metrics for Dynamic wireless charging (1 km), with drivers D1 and D2 on supplied and unsupplied path. Error bars indicate ± one standard deviation.

Overall, the dynamic results are consistent with the physical model of WPT coupling. The measurements extrapolated from the powered lane dominate those from the unpowered lane, and variability increases in the presence of transmitters during movement. Finally, the difference between drivers is visible but secondary to the effect of power supply, and manifests itself mainly as a variation in profile regularity rather than in absolute peaks. At the operating frequency (~86 kHz), all dynamic measurements evaluated via the reconstructed $|B|$ and the average RMS $\langle B_{\text{RMS}} \rangle$ remained within the general public reference levels for magnetic-flux density defined by ICNIRP (2010/2020) and IEEE C95.1-2019, with no exceedances at interior or exterior points. Table I highlight all reference exposure limits for magnetic flux density at 85 kHz, highlighting that the measurements performed are compliant with them [1], [3]–[5], [14].

The proposed workflow is directly transferable to other WPT systems and supports both regulatory compliance evaluations and operational design decisions. Across the tested scenarios, no significant transients or atypical behaviors were detected. Results agree with the coupling physics and the anticipated operating profile, and they comply with the relevant magnetic flux density exposure limits.

IV. Conclusions

This work presented an in-situ measurement campaign of the magnetic field generated by a WPT system for EVs installed at the "Arena del Futuro," including static and dynamic scenarios. Simple and reproducible static indicators (B_{min}, B_{mean}, B_{peak},

979-8-3315-8138-1

TABLE I
REFERENCE EXPOSURE LIMITS FOR MAGNETIC FLUX DENSITY AT 85 kHz.

Standard	Application area	Frequency range	Quantity	Limit at 85 kHz [mT]
ICNIRP 2010 (LF)	General public	3 kHz–10 MHz	B_{rms}	0.027
ICNIRP 2010 (LF)	Occupational	3 kHz–10 MHz	B_{rms}	0.100
IEEE C95.1–2019	Unrestricted environment, head and torso	3.35 kHz–5 MHz	B_{rms}	0.205
IEEE C95.1–2019	Restricted environment, head and torso	3.35 kHz–5 MHz	B_{rms}	0.615
IEEE C95.1–2019	Limbs (public or workers)	3.35 kHz–5 MHz	B_{rms}	1.130
SAE J2954 / IEC 61980	Accessible areas near EV/WPT	~85 kHz	—	adopts ICNIRP/IEEE (commonly 0.027)

std and $B_{\text{RMS,avg}}$) and a consistent data reconstruction flow were defined, allowing direct comparisons between test positions and conditions. The external static results show a clear geometric gradient around the vehicle, with limited dispersion and reduced peak-to-average differences, demonstrating the stability of the operating conditions and constant coupling over time. The internal measurements are lower by an order of magnitude, confirming the combined effects of distance and vehicle shielding on the field. These maps provide useful data for the design of shielding and for the positioning of sensors in verification activities. The dynamic conditions showed a marked separation between the powered and unsupplied sections on all metrics - B_{mean} goes from 5.4÷6.5 μT to 0.28÷0.30 μT, similarly $B_{\text{RMS,avg}}$ goes from 1.9÷2.1 μT to 0.10 μT. The standard deviations also increase significantly on the powered section, consistent with the periodicity of the transmitters and the dynamics of driving. Differences between drivers are present but secondary to the effect of power supply and manifest themselves more as variations in profile regularity (std) than as absolute peaks. These indicators quantify the impact of infrastructure on the exposure profile, maintaining a direct link with the actual composting of the system. The proposed methodology constitutes a procedure that can be transferred to other WPT systems, facilitating compliance checks and operational design. The measurements did not reveal any pronounced transients or behavioral anomalies under the conditions tested. The results are consistent with the physical coupling model and with the system's operating expectations, in full compliance with the standards limiting magnetic flux density.

REFERENCES

[1] ICNIRP, ''Guidelines for limiting exposure to time-varying electric and magnetic fields (1 hz–100 khz),'' 2010.

[2] ICNIRP, ''Guidelines for limiting exposure to electromagnetic fields (100 khz to 300 ghz),'' *Health Physics*, vol. 118, no. 5, pp. 483–524, 2020.

[3] ''IEEE standard for safety levels with respect to human exposure to electric, magnetic, and electromagnetic fields, 0 hz to 300 ghz,'' 2019.

[4] ''SAE J2954: Wireless power transfer for light-duty plug-in/electric vehicles and alignment methodology,'' 2020. Use specific revision year if required.

[5] ''IEC 61980: Wireless power transfer systems for electric vehicles (part 1/2/3),'' 2020. Specify part numbers and publication years as needed.

[6] T. Campi, S. Cruciani, V. De Santis, F. Maradei, and M. Feliziani, ''Wireless power transfer (wpt) system for an electric vehicle (ev): how to shield the car from the magnetic field generated by two planar coils,'' *Wireless Power Transfer*, vol. 5, no. 1, pp. 1–8, 2018.

[7] S. Cruciani *et al.*, ''Innovative passive/active/hybrid shielding solutions for ev wireless charging,'' *Energies*, vol. 16, no. 3822, 2023.

[8] D. D. Lewis, O. A. Badewa, O. Onar, M. Mohammad, J. F. Eastham, and D. M. Ionel, ''Overview of electrically conductive and active shielding for wireless power transfer with a polyphase wireless electric vehicle charging study,'' in *Proc. IEEE Energy Conversion Congress and Exposition (ECCE)*, pp. 1731–1735, 2023.

[9] A. Canova *et al.*, ''Innovative shielding technique for wireless power transfer systems,'' *IET Power Electronics*, 2024.

[10] M. Longo, M. Brenna, D. Zaninelli, C. G. Colombo, A. Curnis, and S. Accinelli, ''Electromagnetic field measurements with dynamic wireless power transfer for charging ev,'' in *IEEE International Conference on Environment and Electrical Engineering and Industrial and Commercial Power Systems Europe (EEEIC / ICPSEurope)*, IEEE, 2025.

[11] ''C95.3-2021 - ieee recommended practice for measurements and computations of electric, magnetic, and electromagnetic fields with respect to human exposure to such fields, 0 hz to 300 ghz,'' 2021.

[12] M. Okada, K. Miwa, S. Kodera, and A. Hirata, ''Compliance assessment of the spatial averaging method for magnetic field leakage from a wireless power transfer system in electric vehicles,'' *Applied Sciences 2024, Vol. 14, Page 2672*, vol. 14, p. 2672, 3 2024.

[13] C. McIntyre, S. Konaklieva, A. B. Nunes, and R. A. McMahon, ''A study of the magnetic field emissions from a vehicle-mounted wireless power transfer system for safe operation when charging ev batteries,'' 2025.

[14] ICNIRP, ''Guidelines for limiting exposure to time-varying electric, magnetic and electromagnetic fields (up to 300 ghz),'' 1998.

979-8-3315-8138-1